Erzincan Üniversitesi
Fen Bilimleri Enstitüsü Dergisi
2025, 18(1), 129-139
ISSN: 1307-9085, e-ISSN: 2149-4584
Araştırma Makalesi

Erzincan University
Journal of Science and Technology
2025, 18(1), 129-139
DOI: 10.18185/erzifbed.1523374
Research Article

Some Physical Attributes of a Cr-Doped Iron Oxide Thin Film Produced by Simultaneous RF and DC Magnetron Sputtering Technique

Günay MERHAN MUĞLU [1], Maryam ABDOLAHPOUR SALARI [2], Volkan ŞENAY [3*], Sevda SARITAŞ [4]

[1]Department of Opticianry, Atatürk University, 25250, Erzurum, Turkey
[2]Department of Physics, Atatürk University, 25250, Erzurum, Turkey
[3*]Department of Opticianry, Bayburt University, 69000, Bayburt, Turkey
[4]Department of Electricity and Energy, Atatürk University, 25250, Erzurum, Turkey

Received: 27/07/2024, **Revised:** 04/12/2024, **Accepted:** 06/01/2025, **Published:** 28/03/2025

Abstract

Iron oxide has recently attracted considerable interest because of its diverse structural and morphological configurations, leading to progressions in various technologies, including ultrahigh magnetic storage, magneto-optical sensors, humidity sensors, and gas sensors. In this research, a thin film of iron oxide doped with chromium was produced on a glass substrate using simultaneous RF and DC magnetron sputtering. The resulting thin film's optical, structural, elemental, and surface characteristics were thoroughly investigated using UV-VIS spectroscopy, XRD, XPS, AFM, and SEM. XRD was utilized to examine the structure of the thin film, which demonstrated good crystallinity. Notably, prominent diffraction peaks at various angles corresponded to specific planes of the normal hematite phase of Fe_2O_3, as verified by the JCPDS Card No. 33-0664. A significant peak at (104) indicated a sturdy development of the hematite phase. The XPS spectrum analysis approved the presence of iron, oxygen, and chromium in the thin film. This study, known for its straightforward methodology, provides valuable insights into the chromium impurity doping process of Fe_2O_3, contributing to a deeper understanding of its structural and morphological characteristics.

Keywords: Fe_2O_3, Cr Doping, RF and DC Magnetron Sputtering Technique

Eşzamanlı RF ve DC Magnetron Saçtırma Tekniği ile Üretilen Bir Cr Katkılı Demir Oksit İnce Filmin Bazı Fiziksel Özellikleri

Öz

Demir oksit, çeşitli yapısal ve morfolojik formları nedeniyle son zamanlarda büyük ilgi görmüş ve ultra yüksek manyetik depolama, manyeto-optik sensörler, nem sensörleri ve gaz sensörleri gibi çeşitli teknolojilerde ilerlemelere yol açmıştır. Bu araştırmada, eşzamanlı RF ve DC magnetron saçtırma kullanılarak bir cam altlık üzerinde krom katkılı ince bir demir oksit filmi üretilmiştir. Ortaya çıkan ince filmin optik, yapısal, elementel ve yüzey özellikleri UV-VIS spektroskopi, XRD, XPS, AFM ve SEM kullanılarak kapsamlı bir şekilde araştırılmıştır. Optik soğurma ölçümlerine dayanarak bant aralığı enerji değeri hesaplandı ve 2,12 eV olarak bulundu. İyi bir kristal yapı gösteren ince filmin yapısını incelemek için X-ışını kırınımı (XRD) kullanılmıştır. JCPDS Kart No. 33-0664 ile doğrulandığı üzere, çeşitli açılardaki göze çarpan kırınım pikleri, Fe_2O_3'ün normal hematit fazının spesifik düzlemlerine karşılık geldiği gözlemlenmiştir. (104) piki, hematit fazının kuvvetli bir şekilde oluştuğunu göstermiştir. XPS spektrum analizi ince filmde demir, oksijen ve kromun varlığını doğrulamıştır. Basit bir metodolojisi ile yürütülen bu çalışma, Fe_2O_3'ün krom safsızlığı katkılama sürecine ilişkin değerli bilgiler sağlayarak yapısal ve morfolojik özelliklerinin daha derinlemesine anlaşılmasına katkıda bulunmaktadır.

Anahtar Kelimeler: Fe_2O_3, Cr katkılama, RF and DC Magnetron Saçtırma Tekniği

*Corresponding Author: vsenay@bayburt.edu.tr
Günay MERHAN MUĞLU, https://orcid.org/0000-0002-4664-1482
Maryam SALARI, https://orcid.org/0009-0002-1199-5632
Volkan ŞENAY, https://orcid.org/0000-0002-6579-2737
Sevda SARITAŞ, https://orcid.org/0000-0002-7274-3968

1. Introduction

Due to its narrow band gap, strong corrosion resistance, non-toxicity, and plenty in the earth's crust, α-Fe_2O_3 is a favorable material [1-5]. Additionally, it is capable of absorbing large quantities of visible light. These properties make it attractive for various applications, including gas-sensitive materials, water photo-oxidation, electrochromism, photocatalysis, interference filters, and solar energy conversion [6, 7]. Recent research indicates that nanostructured α-Fe_2O_3 thin films are suitable for developing hybrid photoelectrodes with multiple junctions, aimed at hydrogen production. [8]. Nevertheless, α-Fe_2O_3 has limited carrier mobility and absorption coefficient [9]. To overcome these limitations, researchers have employed elemental doping, including Cr doping, which has shown promise in enhancing its electronic and optical properties. Cr incorporation introduces structural modifications and alters electronic configurations, potentially improving the material's efficiency in applications such as photocatalysis and photoelectrochemical systems. Various techniques are used to address these constraints, including the use of nanoparticles and elemental doping [10-12].

Spray pyrolysis [13, 14], magnetron sputtering [15, 16], molecular beam epitaxy (MBE) [17], sol-jel [18, 19], chemical vapor deposition (CVD) [20, 21], pulsed laser deposition (PLD) [22], spin coating [23, 24] and electrodeposition [25] are some of the techniques used to produce doped and undoped α-Fe_2O_3 thin films. Among these, magnetron sputtering has garnered significant interest in recent decades due to its economic feasibility and capacity to apply thin films onto diverse substrates for industrial use. In this research, the optical, structural, elemental, and surface attributes of a thin Cr-doped α-Fe_2O_3 film deposited using RF and DC magnetron co-sputtering techniques have been investigated. In this study, the optical, structural, elemental, and surface properties of a Cr-doped α-Fe_2O_3 thin film fabricated using RF and DC magnetron co-sputtering are investigated, offering novel insights into the material's potential enhancements through doping. To the best of our knowledge, limited research exists on Cr-doped α-Fe_2O_3 thin films produced by this technique, adding to the novelty of the present work.

2. Material and Methods

In this research, the RF and DC magnetron co-sputtering technique was used to deposit a Cr-doped α-Fe_2O_3 thin film on a glass microscope slide at a substrate temperature of 400°C. Two-inch Fe (99.99% purity) and Cr (99.99% purity) sputtering targets were installed in two sputtering guns located at the bottom of the vacuum chamber. A DC sputtering voltage of 75 W was applied to the Cr target, while an RF power of 150 W was applied to the Fe target. The distance between each target and the substrate holder was 57 mm, positioned at the summit of the vacuum chamber. During deposition, the substrate spinning was set to 3 rpm. The vacuum

*Corresponding Author: vsenay@bayburt.edu.tr
Günay MERHAN MUĞLU, https://orcid.org/0000-0002-4664-1482
Maryam SALARI, https://orcid.org/0009-0002-1199-5632
Volkan ŞENAY, https://orcid.org/0000-0002-6579-2737
Sevda SARITAŞ, https://orcid.org/0000-0002-7274-3968

chamber pressure was reduced to 3.5×10^{-6} Torr using a mechanical pump and a turbo molecular pump. High-purity (99.99%) Ar gas was then introduced into the sputtering chamber, maintaining an environment pressure of 8.2×10^{-3} Torr throughout the deposition process with an Ar flow rate of 41 standard cubic centimeters per minute and 4 standard cubic centimeters per minute (sccm) O_2. The film thickness was monitored using a thickness monitor during deposition. The deposition process lasted for fifty minutes. These film parameters have been optimized based on our previous research [26, 27]. This study focuses on demonstrating feasibility rather than parameter optimization.

The Cr-doped α-Fe_2O_3 thin film obtained in this study was analyzed using UV-VIS spectroscopy, X-ray photoelectron spectroscopy (XPS), X-ray diffraction (XRD), atomic force microscopy (AFM), and scanning electron microscopy (SEM). To examine the structure of the thin film, an XRD study was conducted using a PANalytical Empyrean system with CuKα1 radiation (λ = 1.5406 Å). XPS measurements were performed at 1486.6 eV X-ray energy using a Specs-Flex system. Surface analysis was carried out using a Zeiss Sigma300 scanning electron microscope (SEM). The surface topography of the thin layer was examined with an AFM 5000II instrument.

3. Results and Discussion

The optical absorption of the resulting film at room temperature was examined over wavelengths ranging from 400 to 900 nm. Fig. 1 illustrates the obtained absorption spectrum. The well-known Tauc equation [28] can be utilized to estimate the energy band gap from the absorption data of the sample.

$$\alpha h\nu = A\left(h\nu - E_g\right)^n \quad (1)$$

Where hν represents the energy of the incident photon, α is the absorption coefficient, and A is a constant related to the energy of the thin film. The parameter n assumes values of 1/2 and 2 for permissible direct and permissible indirect transitions, respectively. The relation below can be used to calculate the absorption coefficient in Equation 1 [29].

$$\alpha = 2.303(A/t) \quad (2)$$

The diagram in Fig. 2 illustrates the relevancy between the square of the absorption coefficient and the photon energy of radiation; the thickness of the film (220 nm) is denoted by t. The intersection point on the horizontal axis represents the band gap energy value of the thin layer. The straight line pattern indicates a direct band gap for the film. The calculated E_g value of 2.12 eV perfectly matches the known energy range of Fe_2O_3.

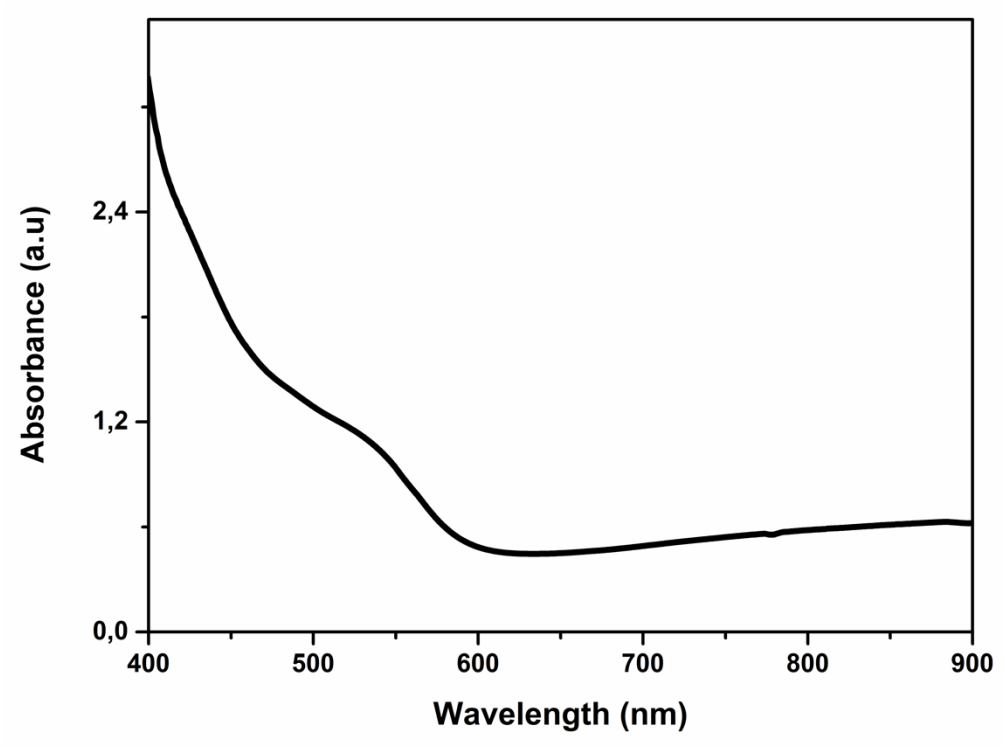

Fig. 1 Absorption spectrum of the produced thin film

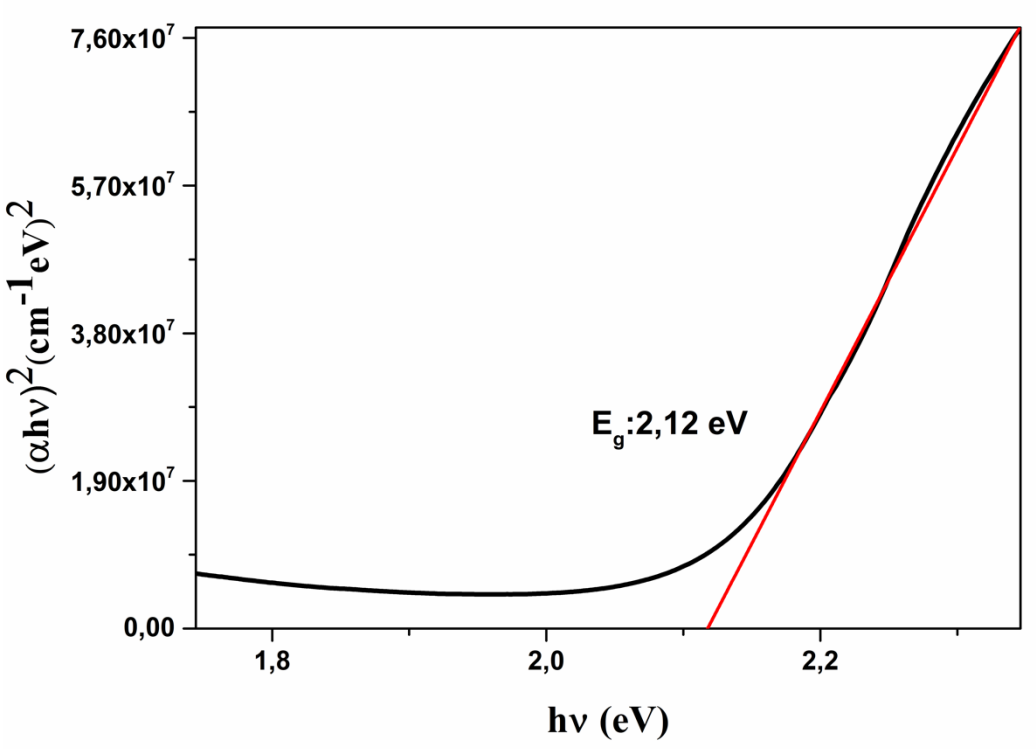

Fig. 2 Band gap of the produced thin film

The structural feature of the obtained thin layer was studied using X-ray diffraction at 2θ angles ranging from 20° to 70°. The resulting XRD pattern is shown in Figure 3. The thin film exhibits a well-defined crystal structure. The (JCPDS Card No. 33-0664) [30-34] confirms that the prominent peaks at approximately 24°, 33°, 36°, 40°, 42°, 55°, and 63° 2θ correspond to the (012), (104), (110), (113), (202), (211), and (214) planes of the normal hematite phase of Fe_2O_3. The peak observed at 50° corresponds to the (211) plane of Cr [35]. The sharpness and intensity of these peaks imply a high degree of crystallinity, which is crucial for optimizing the material's functional properties. Such structural insights are essential for correlating the crystal orientation with the material's potential applications in areas like photocatalysis, gas sensing, and magnetic devices.

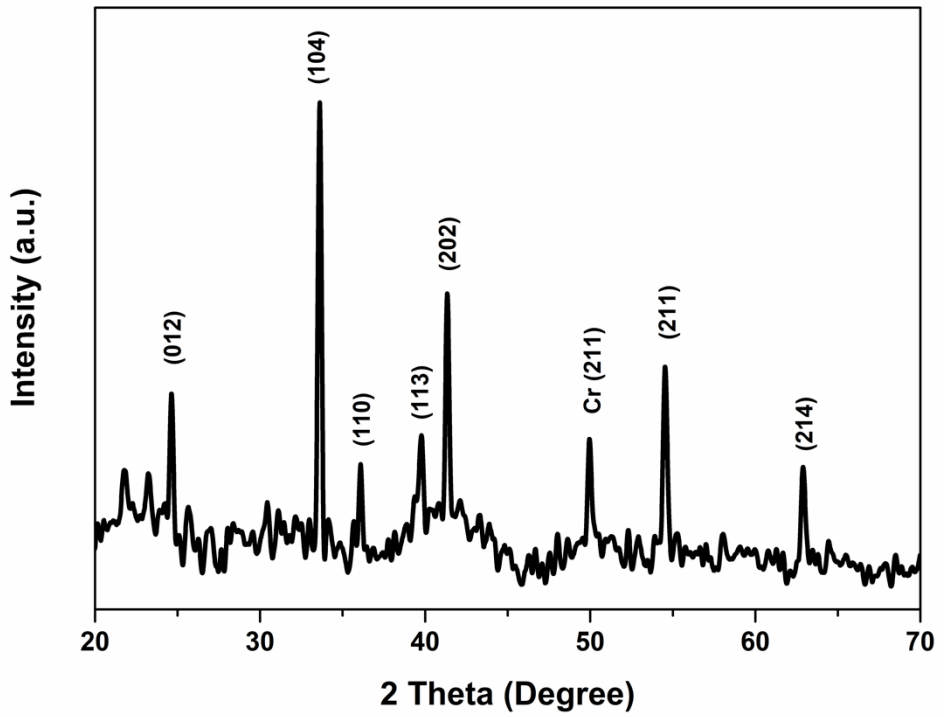

Fig. 3 XRD pattern of the produced thin film

XPS analysis was employed to examine the electronic properties of the Cr-doped Fe_2O_3 thin film. The obtained spectrum (Figure 4) reveals the presence of Fe, O, and Cr in the film. Prominent signals observed include O 1s, Cr 2p3/2, Cr 2p1/2, Fe 2p3/2, Fe 2p1/2, and Fe LMM. Peaks at 707 eV and 721 eV correspond to Fe 2p3/2 and Fe 2p1/2, respectively. The energy difference of 14 eV between Fe 2p3/2 and Fe 2p1/2 is consistent with literature values [36]. These peak positions are characteristic of the Fe^{3+} state in Fe_2O_3 [37]. The O1 spectrum exhibited a peak at 588 eV, representing oxygen atoms in α-Fe_2O_3. According to the XPS results, the elemental atomic percentages of Fe, O, and Cr were determined to be 38%, 60%, and 2%, respectively.

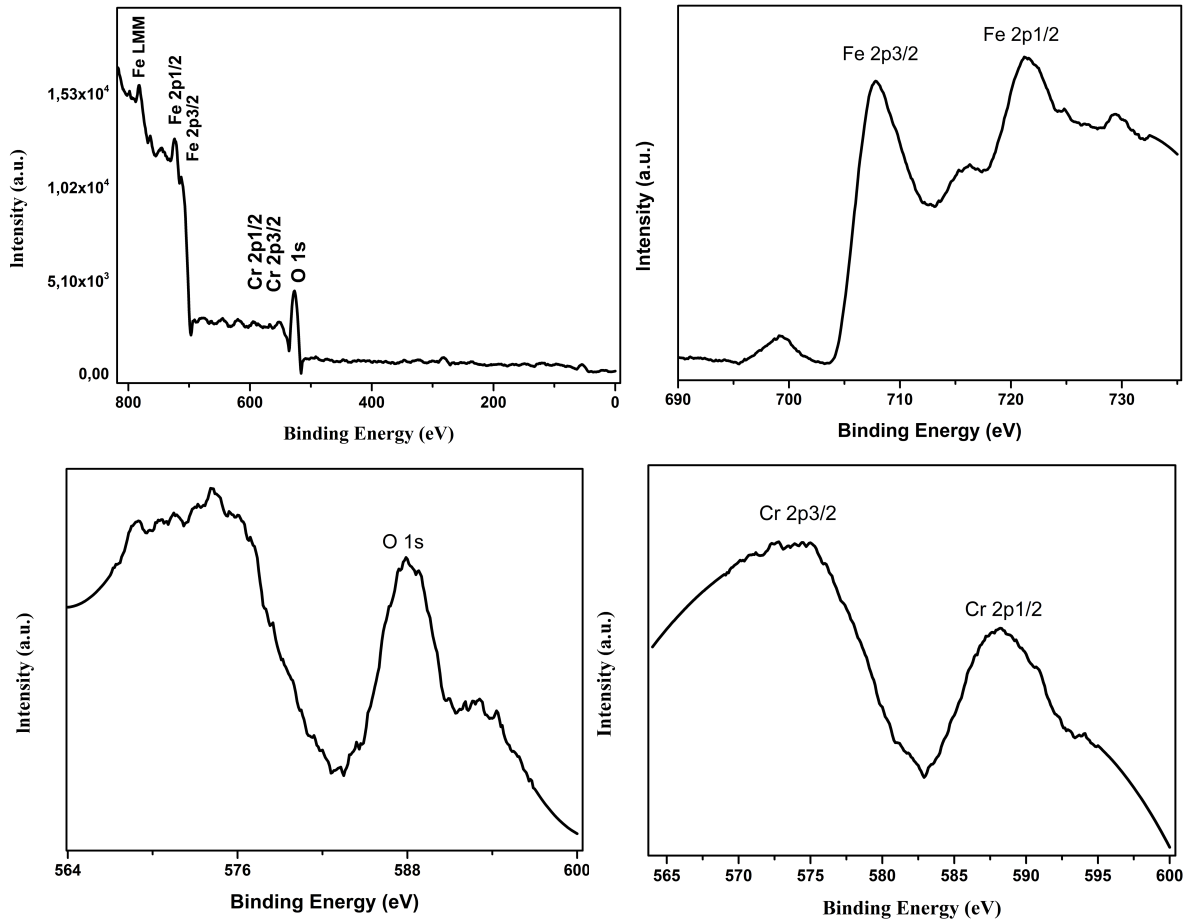

Fig. 4 XPS spectra of the produced thin film

Fig. 5 shows the SEM image at 30,000x magnification, corresponding to the surface morphology of the thin layer deposited onto the glass substrate. The image indicates that the film has a structure with uniformly sized crystals. It also reveals a continuous, homogeneous, and dense film surface without voids or cracks. To calculate the grain size from the top-view SEM image with well-defined grains and the 300 nm scale bar, the grain size can be estimated by measuring the diameters of multiple grains relative to the scale bar. Based on SEM analysis, the calculated average crystallite size is approximately 50 nm. In a scanning electron microscopy (SEM) image, the white and gray areas represent different levels of electron signal intensity, which can provide important information about the sample's composition and topography. The brightness of areas in the SEM image is influenced by the angle at which the sample's surface reflects electrons. Areas facing the detector directly may appear brighter (white), while areas at steeper angles or shadowed regions appear darker (gray). Differences in atomic number can also affect brightness. Higher atomic number elements tend to scatter electrons more effectively, resulting in brighter regions. Conversely, lower atomic number materials scatter electrons less efficiently, appearing darker. In some cases, non-conductive materials can accumulate charge under the electron beam, leading to local brightness variations.

Thicker or denser areas of the sample may reflect or scatter more electrons, appearing brighter compared to thinner or less dense regions. By analyzing the contrast between the white and gray areas, researchers can infer information about the surface morphology, composition, and other material properties.

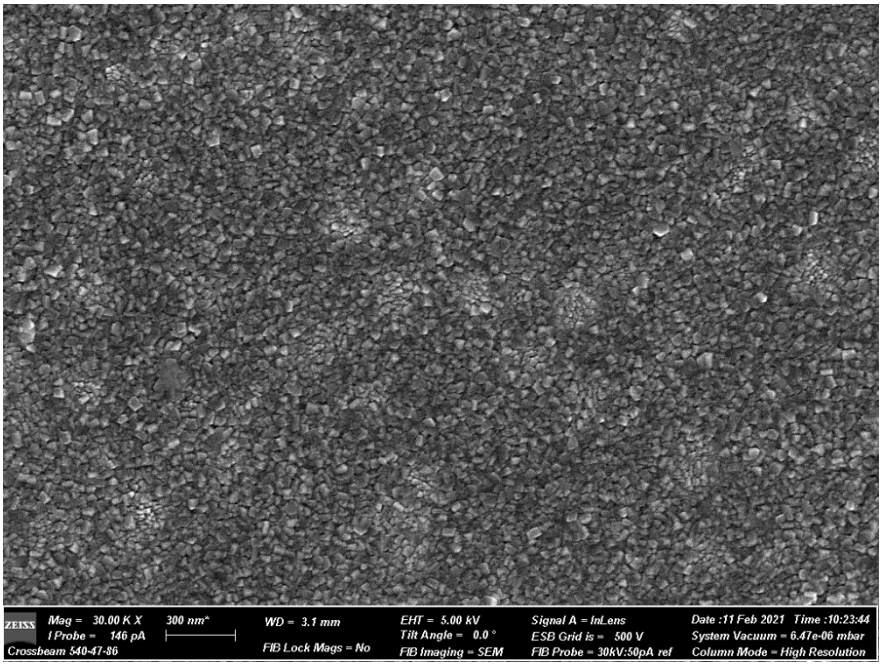

Fig. 5 SEM image of the produced thin film

The surface topography of the thin layer was analyzed using AFM, as depicted in Fig. 6 Surface roughness is crucial for charge transport in thin films and significantly influences the properties of any interfacial layers in device applications. Two-dimensional AFM micrographs exhibit considerable similarity with SEM images. In the three-dimensional representation, needle-like structures are observed on the surface of the thin layer. Additionally, the images indicate the absence of particle clusters on the thin film surface. RMS, which stands for root mean square, quantifies surface roughness by averaging the square root of microscopic peaks and valleys across surfaces. In this film, the RMS surface roughness measures around 2.2 nm. This indicates that the Cr-doped Fe_2O_3 film possesses a smooth surface.

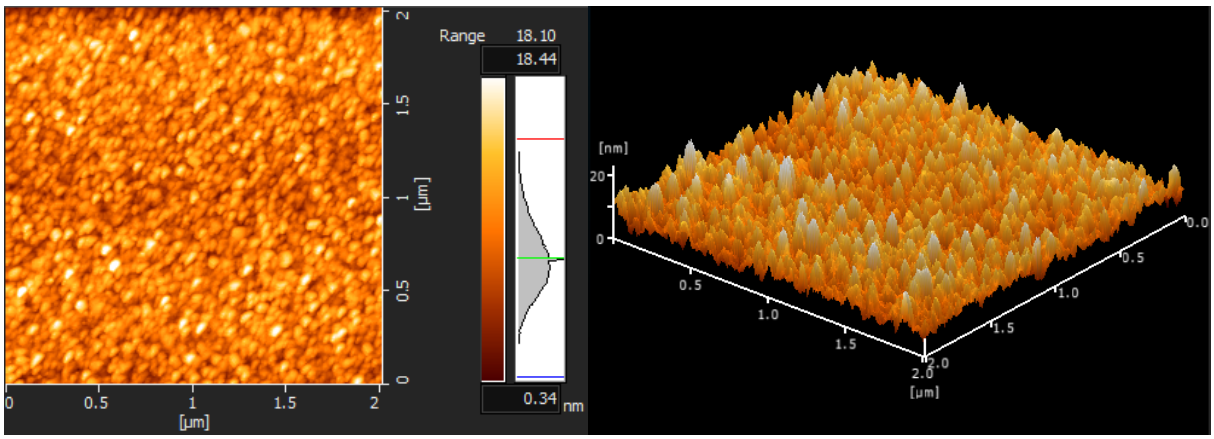

Fig. 6 AFM image of the produced thin film

4. Conclusion

In this research, optical, elemental, structural, and surface attributes of a Cr-doped α-Fe_2O_3 thin layer generated via RF and DC magnetron co-sputtering technique were investigated. It was observed that the thin film exhibits a well-defined crystal structure. In the XRD pattern, a prominent (104) peak indicates the strong presence of the hematite phase, highlighting its significance in the crystal structure of the thin film. The calculated band gap of 2.12 eV matches precisely with the known energy range of Fe_2O_3. XPS analysis was employed to examine the electronic properties of the Cr-doped Fe_2O_3 thin film, showing the Fe, O, and Cr presence in the film. This study may contribute to understanding the doping process of Fe_2O_3 with Cr impurities. The findings verify the chemical states and composition of the elements in the thin film. SEM imaging reveals that the film has a homogeneous and dense surface with uniformly sized crystals, and no voids were observed. Based on analysis, the average crystallite size of the film was obtained to be approximately 50 nm, indicating a stable structure and homogeneous crystal growth. AFM images confirm the absence of particle clusters on the film surface. The RMS value representing surface roughness was approximately 2.2 nm for this specific film, indicating that the Cr film exhibits a highly smooth surface.

Ethics in Publishing

There are no ethical issues regarding the publication of this study.

Author Contributions

Günay MERHAN MUĞLU: Writing–review & editing, Writing–original draft, Investigation, Conceptualization. Maryam ABDOLAHPOUR SALARI: Writing–review & editing, Writing–original draft, Investigation, Conceptualization. Volkan ŞENAY: Writing–review & editing, Writing–original draft, Investigation, Conceptualization. Sevda SARITAŞ: Writing–review & editing, Writing–original draft, Investigation, Conceptualization.

References

1. Abdulnabi, G. and A.M. Juda, Characterization and synthesis of α-Fe2O3 nanoparticles and α-Fe2O3/CuO nanocomposite by hydrothermal method and application them in a solar cell. Journal of Survey in Fisheries Sciences, 2023. **10**(3S): p. 4224-4234.

2. Ateş, T., et al., Ni Katkısının Fe2O3'ün Yapısal Özellikleri Üzerine Etkilerinin Araştırılması. International Journal of Innovative Engineering Applications, 2021. **5**(2): p. 81-87.

3. Domacena, A.M.G., C.L.E. Aquino, and M.D.L. Balela, Photo-Fenton degradation of methyl orange using hematite (α-Fe2O3) of various morphologies. Materials Today: Proceedings, 2020. **22**: p. 248-254.

4. Haridas, V., et al., Ultrahigh specific capacitance of α-Fe2O3 nanorods-incorporated defect-free graphene nanolayers. Energy, 2021. **221**: p. 119743.

5. Mizuno, S. and H. Yao, On the electronic transitions of α-Fe2O3 hematite nanoparticles with different size and morphology: Analysis by simultaneous deconvolution of UV–vis absorption and MCD spectra. Journal of Magnetism and Magnetic Materials, 2021. **517**: p. 167389.

6. Xu, Y., et al., Synthesis and characterization of single-crystalline α-Fe2O3 nanoleaves. Physica E: Low-dimensional Systems and Nanostructures, 2009. **41**(5): p. 806-811.

7. Popov, N., et al., Influence of low-spin Co3+ for high-spin Fe3+ substitution on the structural, magnetic, optical and catalytic properties of hematite (α-Fe2O3) nanorods. Journal of physics and chemistry of solids, 2021. **152**: p. 109929.

8. Miller, E.L., et al., Development of reactively sputtered metal oxide films for hydrogen-producing hybrid multijunction photoelectrodes. Solar energy materials and solar cells, 2005. **88**(2): p. 131-144.

9. Emin, S., et al., Photoelectrochemical water splitting with porous α-Fe2O3 thin films prepared from Fe/Fe-oxide nanoparticles. Applied Catalysis A: General, 2016. **523**: p. 130-138.

10. Annamalai, A., et al., Bifunctional TiO2 underlayer for α-Fe 2 O 3 nanorod based photoelectrochemical cells: enhanced interface and Ti 4+ doping. Journal of Materials Chemistry A, 2015. **3**(9): p. 5007-5013.

11. Hu, Y.-S., et al., Pt-doped α-Fe2O3 thin films active for photoelectrochemical water splitting. Chemistry of Materials, 2008. **20**(12): p. 3803-3805.

12. Wang, L., C.-Y. Lee, and P. Schmuki, Ti and Sn co-doped anodic α-Fe2O3 films for efficient water splitting. Electrochemistry communications, 2013. **30**: p. 21-25.

13. Kumar Pathak, D., et al., Raman area-and thermal-mapping studies of faceted nano-crystalline α-Fe2O3 thin films deposited by spray pyrolysis. Canadian Journal of Chemistry, 2022. **100**(7): p. 507-511.

14. Abedi, S.P., M.B. Rahmani, and F. Rezaii, α-Fe2O3 thin films deposited by a facile spray pyrolysis technique for enhanced ethanol sensing. Physica Scripta, 2023. **98**(5): p. 055901.

15. Huang, M.-C., et al., Magnetron sputtering process of carbon-doped α-Fe2O3 thin films for photoelectrochemical water splitting. Journal of Alloys and Compounds, 2015. **636**: p. 176-182.

16. Ma, Y., et al., The growth mode of α-Fe2O3 thin films by DC magnetron sputtering. Vacuum, 2021. **194**: p. 110625.

17. Zhao, B., et al., Electrical transport properties of Ti-doped Fe 2 O 3 (0001) epitaxial films. Physical Review B—Condensed Matter and Materials Physics, 2011. **84**(24): p. 245325.

18. Yin, S., et al., Tailored fabrication of quasi-isoporous and double layered α-Fe2O3 thin films and their application in photovoltaic devices. Chemical Engineering Journal, 2023. **455**: p. 140135.

19. Khan, U., et al., Ferromagnetic properties of Al-doped Fe2O3 thin films by sol-gel. Materials Today: Proceedings, 2015. **2**(10): p. 5415-5420.

20. Sharma, B. and A. Sharma, Enhanced surface dynamics and magnetic switching of α-Fe2O3 films prepared by laser assisted chemical vapor deposition. Applied Surface Science, 2021. **567**: p. 150724.

21. Zhang, Y.-F., et al., Enhanced visible-light photoelectrochemical performance via chemical vapor deposition of Fe2O3 on a WO3 film to form a heterojunction. Rare Metals, 2020. **39**(7): p. 841-849.

22. Cao, J., et al., Photoanodic properties of pulsed-laser-deposited α-Fe2O3 electrode. Journal of Physics D: Applied Physics, 2010. **43**(32): p. 325101.

23. Grine, A., et al., Effect of precursor concentration and annealing temperature on the structural, optical and electrical properties of pure α-Fe2O3 thin films elaborated by the spin-coating method. Materials Chemistry and Physics, 2022. **276**: p. 125367.

24. Mainali, P., et al., Humidity induced resistive switching and negative differential resistance in α-Fe2O3 porous thin films. Sensors and Actuators A: Physical, 2023. **362**: p. 114631.

25. Rahman, G. and O.-S. Joo, Electrodeposited nanostructured α-Fe2O3 thin films for solar water splitting: Influence of Pt doping on photoelectrochemical performance. Materials Chemistry and Physics, 2013. **140**(1): p. 316-322.

26. Salari, M. A., Muğlu, G. M., Şenay, V., Sarıtaş, S., & Kundakçı, M. (2024). Analysis of optical, structural, and morphological properties of a Ti-doped α-Fe2O3 thin film produced through RF and DC magnetron Co-sputtering. Ceramics International, 50(20), 39221-39225.

27. Sarıtaş, S., Muğlu, G. M., Turgut, E., Kundakçı, M., Yıldırım, M., & Şenay, V. (2024). Optical, structural, morphological, and gas sensing properties of Mg-doped α-Fe2O3 thin films deposited by RF and DC magnetron Co-sputtering technique. Physica B: Condensed Matter, 677, 415704.

28. Tauc, J., R. Grigorovici, and A. Vancu, Optical properties and electronic structure of amorphous germanium. physica status solidi (b), 1966. **15**(2): p. 627-637.

29. Şenay, V., et al., ZnO thin film synthesis by reactive radio frequency magnetron sputtering. Applied Surface Science, 2014. **318**: p. 2-5.

30. S. Mokhtari, et al., Influence of pretreatment on the properties of α-Fe2O3 and the effect on photocatalytic degradation of methylene blue under visible light, Water Sci. Technol. 82 (11) (2020) 2415–2424.

31. P. More, et al., Spray synthesized hydrophobic α-Fe 2 O 3 thin film electrodes for supercapacitor application, J. Mater. Sci. Mater. Electron. 28 (2017) 17839–17848.

32. M. Li, et al., Facile fabrication of three-dimensional fusiform-like α-Fe2O3 for enhanced photocatalytic performance, Nanomaterials 11 (10) (2021) 2650.

33. Dayanand, et al., Deposition of single phase polycrystalline α-Fe2O3 thin film on silicon and silica substrates by spray pyrolysis, Silicon 13 (2021) 3361–3366.

34. J. Tian, et al., Binding Fe 2 O 3 nanoparticles in polydopamine-reduced graphene as negative electrode materials for high-performance asymmetric supercapacitors, J. Nanoparticle Res. 21 (2019) 1–12.

35. Quan, C. and Y. He, Properties of nanocrystalline Cr coatings prepared by cathode plasma electrolytic deposition from trivalent chromium electrolyte. Surface and Coatings Technology, 2015. **269**: p. 319-323.

36. Zhao, P., et al., Facile hydrothermal fabrication of nitrogen-doped graphene/Fe2O3 composites as high performance electrode materials for supercapacitor. Journal of alloys and compounds, 2014. **604**: p. 87-93.

37. Jiang, Z., et al., Natural carbon nanodots assisted development of size-tunable metal (Pd, Ag) nanoparticles grafted on bionic dendritic α-Fe2O3 for cooperative catalytic applications. Journal of materials chemistry A, 2015. **3**(46): p. 23607-23620.